OPTIMISATION OF THE CALIBRATION PROCESS OF A K-TLS BASED MULTI-SENSOR-SYSTEM BY GENETIC ALGORITHMS

J. Hartmann*, I. von Gösseln, N. Schild, A. Dorndorf, J.-A. Paffenholz, I. Neumann

Geodetic Institute, Leibniz University Hannover, Germany -
(hartmann, vongoesseln, dorndorf, paffenholz, neumann)@gih.uni-hannover.de, n.schild@stud.uni-hannover.de

Commission I, WG I/9

KEY WORDS: Kinematic Laser Scanning, (Geo-)referencing, Calibration, Optimisation, Genetic Algorithm

ABSTRACT:

In recent years, the requirements in the industrial production of elongated objects, e.g., aircraft, have been increased. An essential aspect of the production process is the 3D object detection as well as the qualitative assessment of the captured data. On the one hand high accuracy requirements with a 3D standard deviation of $\sigma_{3D} = 1\,mm$ have to be fulfilled, on the other hand an efficient 3D object capturing is needed. In terms of efficiency, kinematic terrestrial laser scanning (k-TLS) has proven its strength in the recent years. It can be seen as an alternative and is even more powerful than to the well established static terrestrial laser scanning (s-TLS). In order to perform a high accurate 3D object capturing with k-TLS, the 3D object capturing of the initial sensor, the (geo-)referencing of the mobile platform, the synchronisation of all sensors and the system calibration, which means the determination of six extrinsic parameters have to be performed with suitable accuracy. Within this contribution we focus on the system calibration. Therefore an approach based on known reference geometries, here planes, is used (Strübing and Neumann, 2013). As a result, the lever arm and boresight angles are determined. Hereby the number as well as the position and orientation of the reference geometries is of importance. Therefore, an optimal arrangement has to be found. Here a sensitive analysis based on uncertainty propagation is used. A selective search of an optimised arrangement is carried out by a genetic algorithm. Within some examples we demonstrate some theoretical aspects and how an optimisation of the reference geometry arrangement can be achieved.

1. INTRODUCTION

In many industrial applications, the 3D object capturing and a quality assurance process is of particular importance. On the one hand a high level of efficiency is needed, on the other hand high accuracy requirements ($\sigma_{3D} = 1\,mm$) have to be achieved. Nowadays, static terrestrial laser scanning (s-TLS) can be seen as a standard procedure. Due to efficiency reasons, the 3D object capturing can be alternatively carried out by kinematic terrestrial laser scanning (k-TLS). In order to fulfil the mentioned high accuracy requirements, a test setup of a k-TLS based multi-sensor-system (MSS), which will be introduced in Section 2.1, is used. Hereby the 3D object is captured by a laser scanner of type Zoller+Fröhlich (Z+F) IMAGER 5016 which fulfils the appropriated accuracy requirements. The (geo-)referencing of the mobile platform is carried out by a laser tracker of type Leica AT960LR in combination with a Leica T-Probe. Because of the fact that the frames of the T-Probe and the laser scanner have different orientations and positions the leverarm and boresight angles have to be determined in a system calibration.

Within this paper, we focus on the procedure and optimisation of a system calibration. The impact of system calibration on the total uncertainty budget of the k-TLS can be very well illustrated by the following calculation example. A deviation of 0.006° in the boresight angles already results in a deviation of $1\,mm$ at a distance of $10\,m$ to the object. This means the boresight angle have to be determined in the range of a few millidegrees. The lever arm instead has to be determined with an accuracy of a few $10^{-1}\,mm$. Thus, it can be seen, that the system calibration provides a significant contribution to the total uncertainty budget of the k-TLS. From this it follows that the system calibration needs a respective consideration, in the context of the entire mapping process. However, a direct determination of the lever arm and the boresight angles is usually difficult or impossible, because the origin and the orientation of an optical sensor (s-frame) are not exactly measurable.

A method to determine the lever arm and boresight angles is to use control points, e.g., marked by artificial targets. This can be, e.g., planar or spherical targets, which have to be well distributed in the object space, see (Vennegeerts, 2011) and (Paffenholz, 2012). These targets are determined by the laser scanner as well as by additional sensors (e.g., total station or a laser tracker). However, the pure usage of ground control points neglects the dimensional information of TLS. Many k-TLS based MSS usually work with laser scanner in a profile mode. This means a determination of 3D control points is often not directly possible. For this reason, a general approach for the determination of the lever arm and boresight angles has to be chosen. An approach was published by (Strübing and Neumann, 2013) and will be presented in detail in Section 2. Further usage and investigations are given in (Keller, 2016), (Heinz et al., 2017) and (Hartmann et al., 2017). The determination of the lever arm and boresight angles will be achieved by measuring known reference geometries with the laser scanner. Due to their simplicity and effectiveness, reference planes (RP) are mostly used and, thus, also considered here. To achieve a high accurate determination of the lever arm and the boresight angles, the arrangement of the RP is of high importance. Calculating all possible RP arrangements is extremely time consuming, though impossible for many RP. Therefore, an optimisation with genetic algorithms (GA) is performed. For a successful optimisation process, a suitable fitness

*Corresponding author

function must be defined to evaluate the quality of a solution (fitness value). Therefore, the standard deviations of the lever arm and boresight angels, which are determined by variance covariance propagation, are used. The main aim of the optimisation is to minimise the standard deviations. Thus, the standard deviations of the lever arm and the boresight angles are combined into a 3D Helmert point error, respectively. For the standard deviations of the boresight angles the distance dependency is taken into account.

In Section 2, we describe the principle of a k-TLS based MSS with the main focus on the system calibration. Furthermore, some theoretical aspects of the RP arrangement are presented. Based on this an optimisation of the system calibration is discussed. Therefore we introduced GA in Section 3. In a first test scenario an optimisation with eight RP of a calibration environment is carried out. The results are shown in Section 4. In Section 5, the results and the benefit of GA based are discussed.

2. THE PRINCIPLE OF K-TLS WITH FOCUS ON THE SYSTEM CALIBRATION

In this section, we first explain the principle of a k-TLS based 3D object capturing. Therefore, a setup of a k-TLS based MSS is introduced. Furthermore, the calibration approach based on RP is discussed in detail. Hereby, the arrangement of the RP is of particular importance for the determination of the lever arm and the boresight angles. Therefore the RP must be orientated and placed in order to be particular sensitive. Based on this the aspect of optimising the process of the system calibration with a GA is discussed.

2.1 A kinematic terrestrial laser scanning based MSS

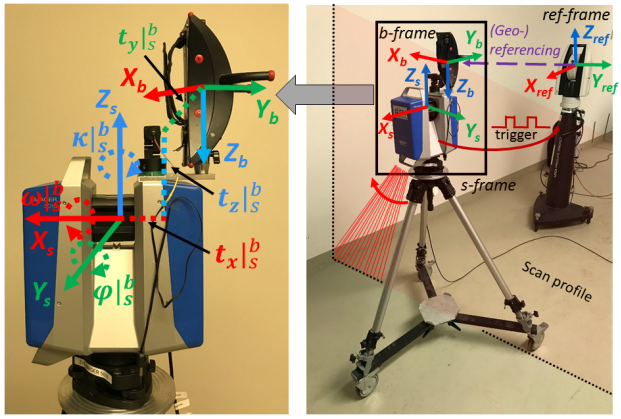

Figure 1. On the left: A detailed view of the sensor and body frame as well as the lever arm and boresight angles. On the right: The principle of the k-TLS based MSS as well as the sensors and their corresponding coordinate frames.

An exemplary setup of a k-TLS based MSS, as further development of (Ehm and Hesse, 2012), as well as the used sensors and their corresponding coordinate frames are shown in Figure 1. The 3D object capturing is carried out by a laser scanner of type Z+F IMAGER 5016 which is mounted on a mobile platform. The laser scanner is operating in the profile mode. For distances less than $10\,m$, accuracies less than $1\,mm$ can be achieved according to the manufacturer specifications, see (Zoller + Fröhlich GmbH, 2018) and (Mettenleiter et al., 2015). A highly accurate determination of the position and orientation of the mobile platform is required for the mentioned measurement tasks. Thus, a laser tracker of type Leica AT960LR in combination with a Leica T-Probe, which is mounted on the laser scanner, is used. The T-Probe has a reference point field, which consist of ten LED's and a reflector. The laser tracker is equipped with a camera, an absolute distance meter and an interferometer. Thus, a six degree of freedom (geo-)referencing measurement to the moving platform is possible. Here three rotations are determined by camera measurements to the LED. The three translations are obtained by the measured horizontal direction, vertical angle and the distance measurement to the reflector. The rotations can be determined with an uncertainty (maximum permissible error) of 0.01° and the translations with $15\,\mu m + 6\,\mu m/m$ (Hexagon Metrology, 2015). The synchronisation of the sensors is achieved by a trigger signal. At the beginning of each profile a pulse is generated by the laser scanner and send to the laser tracker. This pulse triggers the laser tracker and a (geo-)referencing measurement is carried out. Thus, the platform is tracked continuously by the laser tracker and an exact assignment of the captured profiles and (geo-)referencing measurements is achieved. Strictly speaking only the first point of each profile is (geo-)referenced exactly. For a high accurate point wise (geo-)referencing the movement of the platform between the laser tracker measurements has to be considered. This is realised by a Kalman filter. Hereby the movement of the platform will be determined and all points of a profile are shifted respectively (Hartmann et al., 2018).

The 3D transformation of each measured single point $\boldsymbol{P}|_s$ from the coordinate frame of the laser scanner (s-frame) into the coordinate frame of the laser tracker (l-frame or mathematically $|_l$), is obtained within two steps:

$$\boldsymbol{P}|_b \;=\; \boldsymbol{t}(x,y,z)|_s^b + \boldsymbol{R}(\kappa,\varphi,\omega)|_s^b \cdot \boldsymbol{P}|_s \qquad (1)$$

The first step (equation 1) is a transformation from the s-frame to the body coordinate frame (b-frame). The b-frame is represented by the T-Probe. Hereby the vector $\boldsymbol{t}|_s^b$ represents the translations (lever arm) in the coordinate directions x, y, z and $\boldsymbol{R}|_s^b$ is the rotation matrix with the three boresight angles κ, φ, ω. The determination of these parameters is accomplished by means of a system calibration in advance, see Section 2.2. The lever arm can be determined with a standard deviation of $\leq 1\,mm$ and the boresight angles with a standard deviation of a few millidegrees, see (Keller, 2016), (Hartmann et al., 2017) and (Heinz et al., 2017).

If the sensors are mounted stable, it can be assumed that the lever arm and the boresight angles are constant for the whole time span of the measurements.

$$\boldsymbol{P}|_l \;=\; \boldsymbol{t}(x,y,z)|_b^l + \boldsymbol{R}(\kappa,\varphi,\omega)|_b^l \cdot \boldsymbol{P}|_b \qquad (2)$$

The second transformation in equation 2 from the b-frame to the l-frame, is realised by the laser tracker, which is similar to the first. Hereby, the translations $\boldsymbol{t}(x,y,z)|_b^l$ and the rotation matrix $\boldsymbol{R}(\kappa,\varphi,\omega)|_b^l$ are used. These translations and rotations are measured by the laser tracker. Additionally, if necessary, a third transformation from the l-frame to a superordinate reference coordinate frame (ref-frame or mathematically $|_{ref}$) can be carried out. If so, known reference points in the ref-frame have to be measured by the laser tracker. Afterwards all transformation parameters can be estimated by a 3D-Helmert transformation.

2.2 Methodology of the reference geometry based calibration approach

The determination of the lever arm and the boresight angles can be divided into the following main steps:

1. Arrangement of k RP in the measuring range of the TLS-based MSS.
2. Determination of k RP parameters in the ref-frame.
3. Measuring of the RP by the TLS-based MSS.
4. Estimation of the lever arm and boresight angles.
    a) Derivation of approximate values for the lever arm and boresight angles.
    b) Set up the functional model.
    c) Set up the stochastic model.

Step 1 varies depending on the task and usage of sensors. The arrangement and the selection of the number k of RP is described in detail in Section 2.3. In step 2 the normal vector $\boldsymbol{n}_{RP}$ and the distance d_{RP} to the origin of the ref-frame are used as parameters for the RP. If the k-TLS-based MSS measures the RP, then the functional relationship can be formulated by using a Gauss-Helmert model (GHM) (cf. Koch.1999). Hereby, the lever arm and the boresight angles are the unknown parameters. The basic idea for the formulation of the functional model is based on the restriction that the residuals $\boldsymbol{r}$ between the measured laser scanner points $\boldsymbol{P}|_s$ and the RP must be zero, which leads to:

$$r_{j,RP_i} = 0 = \boldsymbol{P}_{j,RP_i}|_{ref} \cdot \boldsymbol{n}_{RP_i} - d_{RP_i} \quad (3)$$
$$\text{with } i = 1, \cdots, k \,;\, j = 1, \cdots, n$$

Hereby n represents the number of respective points per RP. The vector $\boldsymbol{P}_{j,RP_i}|_{ref}$ consist of the transformed point $\boldsymbol{P}_{j,RP_i}|_s$ into the ref-frame, which was measured by the k-TLS based MSS, see Section 2.1. In the adjustment the residuals of the captured laser scanner points and the RP are minimised, till a stop criterion of $0.1\,mm$ for the lever arm and 0.1 millidegrees is reached. It is noteworthy, that the parameters of the RP are estimated values and they can be introduced into the GHM as observations. In this case, a transition to the original observations would be desirable. Because of the complexity and the numerical handling, this is neglected here.

Additionally to the functional model, a stochastic model has to be defined. Therefore, the uncertainties of the observations have to be specified. For a better quantification of the uncertainties, an uncertainty analysis according to the guide to the expression of uncertainty in measurement (GUM) ISO 1995 (JCGM, 2008) is recommended. The variance covariance matrix (VCM) $\boldsymbol{\Sigma}_{ll}$ of the single (derived) observation blocks is given by:

$$\boldsymbol{\Sigma}_{ll} = \begin{bmatrix} \boldsymbol{\Sigma}_{ll}|_s & 0 \\ 0 & \boldsymbol{\Sigma}_{ll}|_b^l \end{bmatrix} = \sigma_0^2 \cdot \boldsymbol{Q}_{ll}, \quad (4)$$

whereby σ_0^2 is the a-priori variance factor and $\boldsymbol{Q}_{ll}$ the cofactor matrix of the observations. $\boldsymbol{\Sigma}_{ll}|_s$ and $\boldsymbol{\Sigma}_{ll}|_b^l$ are representing the VCM of respective observation blocks, which are defined as

$$\boldsymbol{\Sigma}_{ll}|_s = diag(\sigma_x^2, \sigma_y^2, \sigma_z^2)|_s \text{ and}$$
$$\boldsymbol{\Sigma}_{ll}|_b^l = diag(\sigma_{t_x}^2, \sigma_{t_y}^2, \sigma_{t_z}^2, \sigma_\kappa^2, \sigma_\varphi^2, \sigma_\omega^2)|_b^l.$$

Where $(\sigma_x^2, \sigma_y^2, \sigma_z^2)|_s$ are the respective variances of the measured coordinates by the laser scanner and $(\sigma_{t_x}^2, \sigma_{t_y}^2, \sigma_{t_z}^2, \sigma_\kappa^2, \sigma_\varphi^2, \sigma_\omega^2)|_b^l$ are the variances of the (geo-)referencing measurement by the laser tracker. A more detailed explanation of the lever arm and boresight angle determination, can be found in (Strübing and Neumann, 2013) and (Hartmann et al., 2017).

2.3 Arrangement and sensitivity of the reference planes

For the unique determination of the lever arm and the boresight angles, a minimal number $k = 3$ of RP is needed. However, a meaningful level of redundancy for the calculation of the lever arm and boresight angles is required. In addition, it can happen that not all calibration parameters can be determined in an optimal way. Depending on the position and orientation of the RP, they are particularly sensitive for one or more of the calibration parameters. For this reason, the system calibration always has to be carried out with more than three differently oriented RP. In figure 2 a constellation of five RP is shown. Thus, a high sensitivity, by at least one RP, for all parameters of the lever arm and the boresight angle is obtained.

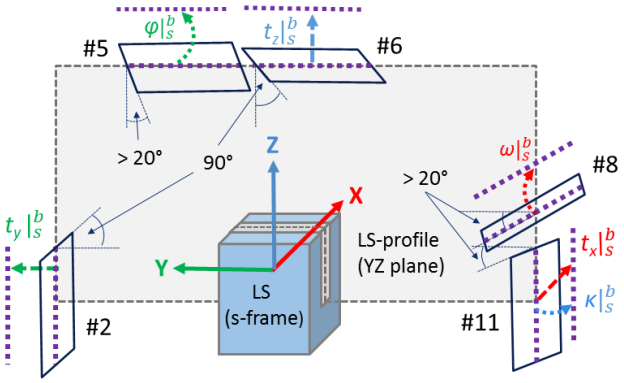

Figure 2. Arrangement of five RP sensitive to the lever arm $(t_x, t_y, t_z)|_s^b$ and boresight angle $(\kappa, \varphi, \omega)|_s^b$.

For both lever arm $(t_x, t_y, t_z)|_s^b$ and boresight angles $(\kappa, \varphi, \omega)|_s^b$ the RP are highly sensitive, if the laser scanner points, are directly shifted out of the RP in the direction of the respective parameter. The presented RP constellation ensures that a change in the respective parameters is directly taken into account in the distance minimisation within the adjustment. That means the RP #2 and #6 are arranged perpendicular to the profile of the laser scanner. For the laser scanner measurements a minimal angle of incidence has to be considered, see, e.g., (Soudarissanane, 2016). Because of this, the RP #5 and #11 are rotated by 20° with respect to the profile of the laser scanner. The RP #8 has to be arranged perpendicular to the laser scanner profile. In addition a rotation of 20° with respect to the XY-plane of the laser scanner has to be carried out. Table 1 shows the arrangement of the five RP.

Table 1. Arrangement of the RP in the laser scanner (LS) frame with respect to the sensitive parameters.

plane	sens. param.	arrangem. to LS profile
#2	$t_y\|_s^b$	$\perp$
#5	$\varphi\|_s^b$	min. $\angle$ 20°
#6	$t_z\|_s^b$	$\perp$
#8	$\omega\|_s^b$	$\perp$ + min. $\angle$ 20° to XY-plane
#11	$(t_x, \kappa)\|_s^b$	min. $\angle$ 20°

The presented RP constellation ensures that the change in the respective lever arm or boresight angle are taken into account in the distance minimisation of the adjustment. That means, larger residuals, see Equation 3, are leading to larger changes of a calibration parameter with respect to a RP, see Figure 2. Another aspect is the minimisation or avoidance of systematic effects. This can be, e.g., false reflections, which are caused by an obtuse angle of incidence or penetration effects in the material by

the laser beam. Thus, a symmetric arrangement of the RP is recommended. That means a unique set up of RP has to be attached at each side equidistant to the laser scanner. In practice, the minimum and maximum measuring distance to the 3D object can be chosen.

2.4 Aim of the optimised arrangement of the reference planes with genetic algorithms

The theoretical aspects of Section 2.3 show that there are some essential things to consider in the arrangement of the RP for a system calibration. It can be summarised that a minimum number $k = 3$ RP is not sufficient for the mentioned high accuracy requirements of the system calibration, see Section 1.

The topic of optimising a system calibration is discussed in (Keller, 2016) and (Heinz et al., 2017). Here, within a simulation, the leverarm and the boresight angles are determined with different RP arrangements and setups of the laser scanner. Furthermore, the standard deviations as well as the correlations of the lever arm and boresight angles are obtained. Based on this the sensitivity of the RP is discussed. In both cases an optimised setup for the system calibration was realised. A similar procedure was carried out at the Geodetic Institute Hannover. Here a Monte Carlo simulation was implemented and the RP were optimised regarding the standard deviations of the lever arm and the boresight angles, see (Dorndorf, 2014). Based on this and with regard to the theoretical aspects, which were explained in Section 2.3, a calibration environment with eleven adjustable RP was installed in a laboratory of the Geodetic Institute Hannover, see Figure 3.

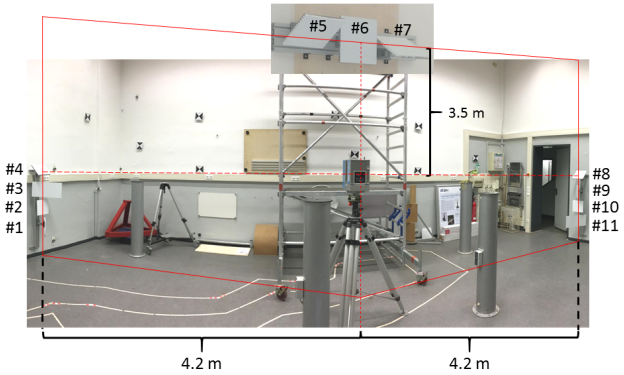

Figure 3. Calibration environment with eleven adjustable reference planes in a laboratory at the Geodetic Institute Hannover.

In total eleven RP are mounted in a profile. At each side of the profile four symmetric arranged RP are mounted. In a system calibration procedure the laser scanner is positioned in the centre of the profile. Thus, the distance at each side is $4.2\,m$. Furthermore, an assembly of three planes is mounted at the ceiling of the lab. Due to the restricted vertical field of view of the used laser scanner model (here Z+F IMAGER 5016) and the unequal dimensions of the lab (height $\sim 5\,m$ and width $\sim 9\,m$) a symmetrical arrangement of further three RP beneath the laser scanner was only partly realised here. In all above mentioned contributions the optimisation of the RP arrangement is based on expert knowledge and carried out in an experimental procedure. A systematical testing of the RP arrangement was not accomplished, because this would have been very time-consuming. However, the optimal solution for the optimisation problem will be surely found. The problem is then solved in a finite number of steps. Here, the complete enumeration, that is, trying out all the solutions is the simplest variant. This method is also called Brute Force Method (BF). The implementation of the BF is often quite simple, but the computational time of the program can increase very fast with a higher complexity. This is even unsolvable for the task of the explained calibration process. This paper focuses on the evaluation and usage of the GA for the calibration process from Section 2.2. An alternative to exact methods are heuristic optimisation methods that examine only a part of the solution space. A successful example of using GA for solving the complex task of scheduling a tachymetric network measurement is given by (von Gösseln, 2017).

In our research, we investigate whether GA, as a heuristic optimisation method, allows a mainly automatic arrangement of the RP in 3D space. GA is a optimisation method that does not require prior knowledge. It is only necessary to set the variables and a fitness function to evaluate the solution quality. The arrangement of each RP in the s-frame is defined by three translations x, y, z and three rotations α, β, γ. At the beginning of the optimisation, all RP can be arranged in a random constellation. The only condition is that all RP must be situated in the profile of the LS. That means, the x-value of the RP is considered as fixed and thus, the values y, z, α, β and γ can theoretically be freely chosen.

For the first tests, we used the calibration environment at the 3D laboratory of the Geodetic Institute Hannover, see Figure 3. A optimisation of a system calibration will be presented in Section 4.

3. GENETIC ALGORITHMS

GA belong to the group of evolutionary algorithms, which are based on the principle of Darwin's biological evolution ("survival of the fittest"). At the beginning of the procedure, a population consisting of a number of individuals is randomly generated. Each individual consists of a sequential sequence of the input parameters (genotype), optional additional information and an individually calculated fitness value (Goldberg, 1989). The genotype stores an encoded version of the proposed solution. The fitness value, which represents the quality of the solution, is determined by a problem-specific evaluation function. To calculate this fitness, the encoded genotype (often binary or permutation encoded) is decoded and converted into the phenotype.

3.1 Functionality of the GA

In GA, several proposals for solutions are treated in parallel, which together form the so-called population (solution set). The initial population P is randomly generated from a fixed number of individuals $numI$. In the progress of optimisation, which is shown in Figure 4, the existing population is modified by the operators *selection*, *crossover* and *mutation*, following Darwin's theory of evolution. The good individuals are selected and participate in the formation of the next generation, the bad individuals survive with less probability. After the selection a crossover (pairing) of two individuals is performed. The subsequent mutation makes small changes to the new individual. The newly created individuals form the next generation of population P'. The process of selection, crossover and mutation is continued until the population P' is full, that means it contains $numI$ individuals. Then $P = P'$ and the process starts again. To complete the optimisation, a suitable abort criterion must be found. This is often a predefined number of generations $numG$. Which values have to be selected for the variables $numI$ and $numG$ strongly depends

on the complexity of the problem. During the optimisation process the best individual is stored in each generation. This allows to create the so-called fitness history.

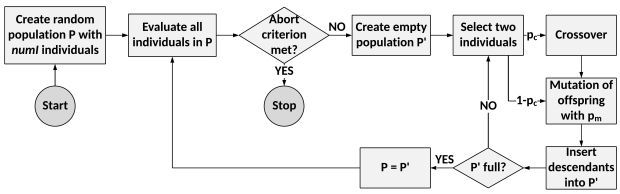

Figure 4. Process of optimisation with GA (according to (Boersch et al., 2007)).

3.2 Operators in GA

To optimise the RP arrangement with GA, we use the **Global Optimization Toolbox** in MATLAB (MathWorks, 2019). Next, the operators of the GA will be briefly explained. For further information see e.g. (Goldberg, 1989).

Selection: The selection process selects a part of the individuals of the population P to create the next generation. Different selection methods have a different selection pressure, which controls the loss of the diversity. In this case, the "stochastic uniform" is used as a selection function. In order to transfer the best individuals of one generation to the next generation in each case, *elitism* is used (MathWorks, 2019). Here, the best individuals of a generation are taken over without any changes into the population of the next generation.

Crossover: After the selection of the individuals, two individuals are crossed with each other with a certain crossover probability (recombination probability) p_c. The crossover operator merges the characteristics of different individuals by combining two parents (selected individuals of the current generation) into two offspring (individuals of the next generation).

Mutation: To preserve diversity, the features of the recombined solutions are randomly changed at one or more locations with a mutation probability p_m. The standard mutation changes the bit coding of the genotype: with a certain mutation probability, one or more bits of the parameter vector are negated.

The described procedure of selection, crossover and mutation is carried out until the abort criterion of a maximum number of generations is met. The individual with the best fitness value is the result of optimisation.

In the next section, we describe which values are assumed as variables in the context of the optimised arrangement of RP. These variables form the double value coded phenotype of the GA. We also set up the fitness function that is used to evaluate the quality of the solution (see Section 4.3).

4. OPTIMISATION OF THE SYSTEM CALIBRATION

In this section an optimisation of the system calibration, which was explained in Section 2, is carried out. This will be done with the RP of the calibration environment at the 3D laboratory of the Geodetic Institute Hannover, see Figure 3. The RP $\#3, \#7$ and $\#9$ are not considered, because of a similar arrangement to the RP $\#1, \#5$ and $\#11$. This reduces the number of possibilities and computing time. The arrangement of the selected eight RP, is shown in Figure 5.

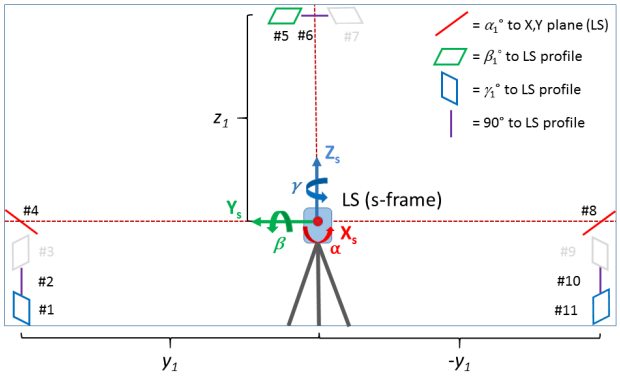

Figure 5. The arrangement of eight selected RP from the calibration environment cf. Figure 3 and the laser scanner in the centre.

Table 2. Positions of the RP with respect to the laser scanner (s-frame).

#plane	x [m]	y [m]	z [m]	α[°]	β[°]	γ[°]
#1	0.0	y_1	-0.8	90	0	$-\gamma_1$
#2	0.0	y_1	-0.4	90	0	0
#4	0.0	y_1	0.0	$-\alpha_1$	0	0
#5	0.0	0.4	z_1	0	0	0
#6	0.0	0.0	z_1	0	β_1	0
#8	0.0	$-y_1$	0.0	α_1	0	0
#10	0.0	$-y_1$	-0.4	90	0	0
#11	0.0	$-y_1$	-0.8	90	0	γ_1
LS	0.0	0.0	0.0			

4.1 Fixed and variable parameters of the optimisation

Within a first test scenario, the arrangement of the eight selected RP of the calibration environment is analysed. Table 2 shows the fixed and variable parameters of the optimisation.

In total there are three RP assemblies. The first (RP $\#1$, $\#2$ and $\#4$) and second (RP $\#8$, $\#10$ and $\#11$) are placed to the left and right of the laser scanner at a distance of y_1 and $-y_1$. The third assembly with the RP ($\#5$ and $\#6$) is placed above the laser scanner with a distance of z_1. All planes are centred in the profile of the laser scanner. Thus, all x-coordinates are set $x = 0\,m$. Here the distance between the laser scanner and the left and right assembly is set identical. This is done have the same magnitude of the mentioned systematic effects, coming from the angle of incidence and penetration depth of laser beam, see Section 2.3. The minimum distance of the laser scanner measurement is set to $1\,m$. A lower measuring distance leads to a higher noise, see (Hartmann et al., 2017). According to the typical measurement scenario for the introduced k-TLS based MSS and the calibration environment, we set $y_1 = 1\,m \ldots 10\,m$ and $z_1 = 1\,m \ldots 4\,m$.

In addition to the horizontal y and vertical z position of the RP assemblies, the rotations α, β, γ of the RP have to be determined. To eliminate the systematic effects, a similar rotation of the opposite planes is chosen here. Thus, an equal angle of incidence on both sides is obtained. The RP $\#1$ and $\#11$ are rotated, e.g., by the angle γ. To avoid a bad angle of incidence the possible rotation ranges from $70°$ to $0°$. At $0°$ the RP are perpendicular to the laser scanner profile.

The RP $\#2$, $\#6$ and $\#10$ are arranged perpendicular to the laser scanner profile in order to be most sensitive for the determina-

Table 3. Bounds and increments of the variables

variable	upper bound	lower bound	increment	possibilities
y_1	$10\,m$	$1\,m$	$0.5\,m$	19
z_1	$4\,m$	$1\,m$	$0.5\,m$	7
α_1	90°	20°	5°	15
β_1	70°	0°	5°	15
γ_1	70°	0°	5°	15
total				448875

tion of the lever arm in the y- and z-direction. All bounds and increments of each variable are shown in Table 3. If a step size of $0.5\,m$ is used for the distances and 5° is used for the rotations of the RP, there are 448875 ways to arrange the RP assembly.

If all five variables are determined in the optimisation, the phenotype of the GA is given by:

$$pt = [y_1\ z_1\ \alpha_1\ \beta_1\ \gamma_1]. \tag{5}$$

In the initial population, random values are generated for the variables of the phenotype within the lower and upper bounds with the respective increment (see Table 3). In total, $numI$ randomly generated individuals form the starting population.

4.2 Application of an optimisation

An optimisation of a system calibration was carried out with the introduced settings in Section 4.1. Therefore the intersection points at each RP with the laser scanner profile were calculated. For a realistic scenario different steps of the resolutions for the zenith angle are possible according to the specifications of the used Z+F IMAGER 5016, see (Zoller + Fröhlich GmbH, 2018). In our optimisation we have chosen the resolution for the zenith angle to high $= 0.036^\circ$. The number of intersection points per RP depends on the resolutions for the zenith angle and the distance. Thus, the distance d, the horizontal direction φ and the vertical angle θ are calculated.

Furthermore, the VCM has to be introduced. This is done according to Equation 4. For the laser scanner measurement the parameters: $\sigma_d = 0.5\,mm$, $\sigma_\varphi = 0.004^\circ$ and $\sigma_\theta = 0.004^\circ$ are chosen. Whereby the standard uncertainty of the distance σ_d consists of the linearity error, which is given by $< 1\,mm$ as well as of the noise of the distance measurement. Here for a distance of $< 10\,m$ a rms of $< 0.3\,mm$ is given, see (Zoller + Fröhlich GmbH, 2018). The standard uncertainties of the measured parameter distance d, horizontal direction φ and the vertical angle θ are converted to the standard uncertainties of the coordinate directions $\sigma_{x,y,z}|_s$ with uncertainty propagation, see (JCGM, 2008). To establish a relationship between the laser scanner (s-frame) and the ref-frame where the RP are given, a six degrees of freedom measurement of the laser tracker (here Leica AT960LR) to the T-Probe is carried out. The distance of the laser tracker to the laser scanner is set to $2\,m$. According to the manufacturer, realistic standard uncertainties of a measurement are half of the given maximum permissible errors, see (Hexagon Metrology, 2015). That means for the rotations $\sigma_{\omega,\varphi,\kappa}|_b^l = 0.005^\circ$ and for the translations $\sigma_{t_{x,y,z}}|_b^l = 7.5\,\mu m + 3\,\mu m/m$. However, these values are still specified as a 3D point uncertainty a. Thus, they have to be converted into a standard uncertainty $u_{x_j} = \frac{1}{\sqrt{3}} \cdot a$, see (JCGM, 2008). This results in the standard uncertainty of $\sigma^2_{t_{x,y,z}}|_b^l < 0.1\,mm$ and $\sigma_{\omega,\varphi,\kappa}|_b^l = 0.002^\circ$.

4.3 Definition of the fitness functions

Within the optimisation of the system calibration with a GA a fitness function must be defined. Here the effects of the lever arm and boresight angles must be taken into account. For the lever arm this is done with the fitness function f_1. This can be seen as a 3D Helmert point error. In case of the boresight angles the 3D point error (f_2) must be calculated with respect to the distance d. Furthermore, a combined fitness function f_3 is defined.

$$f_1 : \sigma_{trans} = \sqrt{(\sigma^2_{t_x} + \sigma^2_{t_y} + \sigma^2_{t_z})|_s^b} \tag{6}$$

$$f_2 : \sigma_{rot,d} = d \cdot \sqrt{(\sigma^2_{\omega} + \sigma^2_{\varphi} + \sigma^2_{\kappa})|_s^b} \tag{7}$$

$$f_3 : \sigma_{trans,rot,d} = \sqrt{\sigma^2_{trans} + \sigma^2_{rot,d}} \tag{8}$$

To evaluate the quality of the calibration process the object distance d is introduced in the fitness function f_2 and f_3. Here $d = 10\,m$ is the usual scan distance in the measurement process; not in the calibration process.

4.4 Test scenarios

To evaluate the suitability of the GA for the arrangement of RP for calibration purposes, the test scenarios in Table 4 are evaluated. We first calculated the fitness function separately for translation effects (f_1) and rotation effects (f_2). In f_3 we used a fitness function that takes the effects of the lever arm as well as the boresight angles into account.

We have gradually increased the number of variables in the optimisation process. First, we introduced the position of the assemblies in the room as variables, y_1 and z_1. For the rotations of the RP we used values of $\alpha_1 = 30^\circ$, $\beta_1 = 45^\circ$ and $\gamma_1 = 45^\circ$. In the first line of Table 4 it can be seen that the number of possibilities in this case (133) is very low and can also be carried out by a BF algorithm within 1.3 hours, when a calculation of a solution in the GHM takes about 35 seconds.

Second, we introduced the rotations of some RP as variables. For the rotation of the RP with the variables α_1, β_1, γ_1 there are already 3375 possibilities. The evaluation of a BF solution would take 32.8 hours. With GA only a part of the solution space is evaluated (here: 20 individuals and 10 generations). This reduces the calculation time to 1.9 hours. Whether this number of individuals is sufficient to determine a good or even optimal arrangement of the RP can be determined by comparing the GA results with the BF solution. Since the BF solution is not available yet, the optimisation was carried out several times. In any case, a comparison with the BF solution is the next step in our work. When optimising the rotations separately, we used the results of the first optimisation for y_1 and z_1 (e.g.,e $f_1 : y_1 = 1.0\,m$ and $z_1 = 4.0\,m$ and $f_2 : y_1 = 3.5\,m$ and $z_1 = 3.0\,m$, see Table 5).

In the third simulation all variables were combined in one optimisation. The number of possibilities then increases to 448875 and the BF computation time would be 4364 hours. With the GA, we reduce the computation time to under 8 hours if only 40 individuals and 20 generations are evaluated.

4.5 Results of the optimisation

The results of the optimisation are shown in Table 5 and 6. At least three runs were performed per fitness function and set of variables. The good repeatability of the achieved results can be

Table 4. Different executed test scenarios

fitness function	variables	poss. BF	numI	numG	poss. GA	computing time[1] per sol. [sec]	GA [hours]	BF [hours]
f_1	y_1, z_1	133	10	10	100	35	1.0	1.3
	$\alpha_1, \beta_1, \gamma_1$	3375	20	10	200	35	1.9	32.8
	$y_1, z_1, \alpha_1, \beta_1, \gamma_1$	448875	40	20	800	35	7.8	4364.1
f_2	y_1, z_1	133	10	10	100	35	1.0	1.3
	$\alpha_1, \beta_1, \gamma_1$	3375	20	10	200	35	1.9	32.8
	$y_1, z_1, \alpha_1, \beta_1, \gamma_1$	448875	40	20	800	35	7.8	4364.1
f_3	y_1, z_1	133	10	10	100	35	1.0	1.3
	$\alpha_1, \beta_1, \gamma_1$	3375	20	10	200	35	1.9	32.8
	$y_1, z_1, \alpha_1, \beta_1, \gamma_1$	448875	40	20	800	35	7.8	4364.1

[1] computer performance: Intel Core i7-3770 (4-cores, 3.40 GHz, 32 GB RAM)

seen in Table 5. This suggests a proper choice of the number of individuals and generations. Due to the heuristic procedure an optimal result can not be guaranteed. For this, a comparison with an exact optimisation method (e.g. BF) is necessary. This step is upcoming and will be completed soon.

When the fitness function f_1 is used, the RP assemblies are unsimilarly positioned at the minimal permissible value $y_1 = 1\,m$ and the maximal permissible value $z_1 = 4\,m$. This is not in accordance with the theory, which assumes an equal distance for the RP assemblies. This behaviour using f_1 will be investigated in further work. A feasible reason could be that the RP in the z direction are only arranged above the laser scanner. In theory the translations can be determined more accurately when the RP assemblies are closer to the laser scanner. In addition, the translation component can be determined more accurately when the angle of incidence on the individual RP is perpendicular, see Figure 2.

When using the fitness function f_2 and f_3, the RP assemblies are positioned at a distance of $y_1 = 3.5\,m$ and $z_1 = 3.0\,m$. The results of f_2 and f_3 are almost identical, which can be explained by the fact that the numerical value of the rotational component (f_2) in the combined fitness function f_3 is almost 20 times larger than that one of the translation components (f_1).

When looking at the rotations of the RP, it can be seen that these are usually in the conceded boundary area. The angle of incidence is very flat for all RP to reach a high sensitivity of the observations. This is not the case for the optimisation with the fitness function f_1. Here the angles of incidence are for most of the RP perpendicular.

Based on the results of the combined optimisation (Table 6), it can be seen that the distance between the RP and the laser scanner in the $y-$direction becomes significantly larger than when optimising the translations separately with predefined rotations of $\alpha_1 = 30^\circ$, $\beta_1 = 45^\circ$ and $\gamma_1 = 45^\circ$. The rotations of the RP are again at the edge of the permissible boundary and have a very flat angle of incidence. The fitness value improves by $0.1\,mm$ with increasing distance between RP and laser scanner. A larger distance of the RP to the laser scanner has a more positive impact on the determination of the boresight angles than a negative impact on the lever arm.

5. CONCLUSION

The impact of the system calibration on the overall uncertainty budget for a 3D object capturing with a k-TLS based MSS can be

Table 5. Results of a separate optimisation of the RP translations and the rotations

fit. func.	run	separate y_1 $[m]$	z_1 $[m]$	fitness $[mm]$	separate α_1 $[^\circ]$	β_1 $[^\circ]$	γ_1 $[^\circ]$	fitness $[mm]$
f_1	1	1.0	4.0	0.04	65	70	60	0.03
	2	1.0	4.0	0.04	65	70	60	0.03
	3	1.0	4.0	0.04	55	70	60	0.03
f_2	1	3.5	3.0	0.67	30	70	70	0.63
	2	3.5	3.5	0.68	30	70	70	0.63
	3	3.5	3.0	0.67	30	70	70	0.63
f_3	1	3.5	3.0	0.67	25	70	70	0.64
	2	3.5	3.0	0.67	30	70	60	0.64
	3	3.5	3.0	0.67	30	70	70	0.64

essential. Thus, special attention is put on the determination of the lever arm and boresight angles by means of reference geometries (here RP). Our current investigations aim at an optimisation of the arrangement of the RP based on the proposal of (Strübing and Neumann, 2013). The goal is to improve the accuracies in the determination of the lever arm and boresight angles, see (Corndorf, 2014), (Keller, 2016) and (Heinz et al., 2017). This optimisation process is carried out with a prior expert knowledge. Within this contribution a systematic optimisation of the system calibration based on GA is developed. As a first test scenario, the arrangement of the calibration environment, located in the 3D laboratory of the Geodetic Institute Hannover, consisting of eight RP is optimised. Therefore, a fitness function is introduced which takes both effects of the lever arm and the boresight angle into account. The distance dependency of the boresight angles is explicitly considered.

For the optimisation process at least three runs per fitness function and set of variables were performed. The results show a good repeatability of the RP arrangement. This suggests a proper choice of the number of individuals and generations. Due to the heuristic procedure an optimal result can not be guaranteed. The calculated fitness values show that a system calibration can be carried out with a sufficient accuracy with respect to our defined accuracy requirement in section 1. Here a few $10^{-1}\,mm$ for the lever arm and a few millidegrees for the boresight angles were demanded. The combined fitness function f_3 accounts for both effects, the lever arm and the boresight angles, in the optimisation. It is noteworthy, that the resulting fitness value is more and more dominated by the boresight angles the larger the distance to

Table 6. Results of a combined optimisation of the RP translations and rotations (i.e. all five variables)

fit. func.	run	combined y_1 $[m]$	z_1 $[m]$	α_1 $[°]$	β_1 $[°]$	γ_1 $[°]$	fitness $[mm]$
f_1	1	1.0	4.0	60	70	70	0.03
	2	1.0	4.0	55	70	70	0.03
	3	1.0	4.0	60	70	65	0.03
f_2	1	8.0	2.5	20	70	70	0.57
	2	8.0	2.5	20	70	70	0.57
	3	8.5	2.5	20	70	70	0.58
f_3	1	8.0	2.5	20	70	70	0.57
	2	8.0	2.5	20	70	70	0.57
	3	8.0	2.5	20	70	70	0.57
	4	8.0	2.5	20	70	70	0.57
	5	8.0	2.5	25	70	70	0.58
	6	6.5	2.5	25	65	65	0.60
	7	8.0	2.5	20	70	70	0.57
	8	8.0	2.5	20	70	70	0.57
	9	8.0	2.5	20	70	70	0.57
	10	8.0	2.5	20	70	70	0.57

the RP is. This can be seen as the more critical part than the lever arm with regard to the overall accuracy requirements. But finally, the high accuracy requirements for a 3D object capturing with a 3D standard deviation of $\sigma_{3D} = 1\,mm$ can be fulfilled.

In further research a more complex consideration of the optimisation of the RP arrangement should be investigated. Hereby, the number of fixed and variable parameters for the arrangement of the RP will be systematically varied. This allows to find new constellations for the positioning of the RP.

ACKNOWLEDGEMENTS

The presented methods and results were obtained in the scope of the collaborative research project „FINISH - Exakte und schnelle Geometrieerfassung sowie Datenauswertung von Schiffsoberflächen für effiziente Beschichtungsprozesse“ and are part of the subproject „Entwicklung von Algorithmen und Qualitätsprozessen für ein neuartiges kinematisches terrestrisches Laserscanningsystem (03SX406D)“, which is funded by the German Federal Ministry for Economic Affairs and Energy (BMWi).

REFERENCES

Boersch, I., Heinsohn, J. and Socher, R., 2007. *Wissensverarbeitung: Eine Einführung in die künstliche Intelligenz für Informatiker und Ingenieure*. 2nd edn, ELSEVIER Spektrum Akademischer Verlag, München.

Dorndorf, A., 2014. *Prozessoptimierung von TLS-basierten kinematischen Mapping-Systemen. Master thesis (unpublished)*. Leibniz University Hannover, Hannover.

Ehm, M. and Hesse, C., 2012. Entwicklung eines kinematischen laserscansystems für anwendungen im schiffbau. In: Fraunhofer IGD (ed.), *Go-3D 2012 Computergraphik für die Praxis*, Vol. 2012, Fraunhofer Verlag, pp. 31–36.

Goldberg, D. E., 1989. *Genetic algorithms in search, optimization, and machine learning*. Addison-Wesley, Boston.

Hartmann, J., Paffenholz, J.-A., Strübing, T. and Neumann, I., 2017. Determination of position and orientation of lidar sensors on multisensor platforms. *Journal of Surveying Engineering* 143(4), pp. 11.

Hartmann, J., Trusheim, P., Alkhatib, H., Paffenholz, J.-A., Diener, D. and Neumann, I., 2018. High accurate pointwise (geo-)referencing of a k-tls based multi-sensor-system. *ISPRS Annals of Photogrammetry, Remote Sensing and Spatial Information Sciences* IV-4, pp. 81–88.

Heinz, E., Eling, C., Wieland, M., Klingbeil, L. and Kuhlmann, H., 2017. Analysis of different reference plane setups for the calibration of a mobile laser scanning system. In: *Lienhart, W. (Hrsg.): Ingenieurvermessung 2017, Beiträge zum 18. Internationalen Ingenieurvermessungskurs, Graz, Austria*, pp. 131–146.

Hexagon Metrology, 2015. Leica absolute tracker at960 (product brochure). www.hexagonmi.com/en-GB/products/laser-tracker-systems/leica-absolute-tracker-at960 (24 March 2019).

JCGM, 2008. Evaluation of measurement data: Guide to the expression of uncertainty in measurement (gum 1995 with minor corrections, iso/iec guide 98-3).

Keller, F., 2016. *Entwicklung eines forschungsorientierten Multi-Sensor-Systems zum kinematischen Laserscanning innerhalb von Gebäuden: PhD thesis*. Shaker Verlag, Aachen.

MathWorks, 2019. Matlab - documentation genetic algorithm. https://de.mathworks.com/help/gads/genetic-algorithm.html (01 April 2019).

Mettenleiter, M., Härtl, F., Kresser, S. and Fröhlich, C., 2015. *Laserscanning: Phasenbasierte Lasermesstechnik für die hochpräzise und schnelle dreidimensionale Umgebungserfassung*. Die Bibliothek der Technik, Vol. Bd. 371, Verl. Moderne Industrie, München.

Paffenholz, J.-A., 2012. *Direct geo-referencing of 3D point clouds with 3D positioning sensors: PhD thesis*. DGK, Reihe C, Vol. 689, München.

Soudarissanane, S., 2016. *The geometry of terrestrial laser scanning; identification of errors, modeling and mitigation of scanning geometry: PhD thesis*. TU Delft, Delft.

Strübing, T. and Neumann, I., 2013. Positions- und Orientierungsschätzung von LIDAR-Sensoren auf Multisensorplattformen. *zfv – Zeitschrift für Geodäsie, Geoinformation und Landmanagement* 138(3), pp. 210–221.

Vennegeerts, H., 2011. *Objektraumgestützte kinematische Georeferenzierung für Mobile-Mapping-Systeme: PhD thesis*. DGK, Reihe C, Vol. 657, München.

von Gösseln, I., 2017. *Simulationsbasierte Effizienzoptimierung von Messprozessen am Beispiel der tachymetrischen Netzmessung: PhD thesis*. DGK, Reihe C, Vol. 800, München.

Zoller + Fröhlich GmbH, 2018. Z+f imager 5016, 3d laser scanner data sheet. www.zf-laser.com/Z-F-IMAGER-R-5016.184.0.html (24 March 2019).

Revised April 2019